The Stanford
Relativity Gyroscope Experiment
(B): Gyroscope Development

J. A. Lipa and G. M. Keiser

1. INTRODUCTION

The central element of the Stanford relativity experiment is a cryogenic
gyroscope with a performance in space many orders of magnitude superior
to that of conventional earth-bound devices. In the early phases of the
program, a great deal of thought was given to the problem of achieving
the performance goal, and an entirely new gyro concept was developed by
William Fairbank and Francis Everitt, based on the application of cryogenic
techniques to electrostatic gyroscopes. In paper VI.3(A) Francis Everitt
has given a history and overview of the experiment. In this paper we
describe the construction of the gyroscope, outline its development into an
operational laboratory device, and present some of the results obtained with
it. We also give a brief account of the torque analysis which demonstrates
that it is feasible to make a gyroscope with the desired performance.

2. GENERAL DESCRIPTION

The gyroscope is an adaptation of the electrically suspended gyroscope
(ESG) invented by A. Nordsieck in 1952 [1] and subsequently developed in

variant forms by Honeywell and Rockwell. The Stanford version of the gyroscope has five main differences from conventional ESG's: (i) an operating temperature of around 2 K, (ii) a gas spin up system, (iii) a superconducting readout system, (iv) ideally equal moments of inertia, and (v) more stringent manufacturing tolerances for the rotor. These differences stem from a number of interwoven requirements placed on the experiment which must be met if the underlying scientific goal is to be achieved. For example, the readout system makes use of the London moment (described in the previous paper) not only because it works so well with a perfectly spherical superconducting rotor, but also because it gives an extremely linear readout, which is essential for calibrating the experiment, and because it is relatively immune to rotor mis-centering errors.
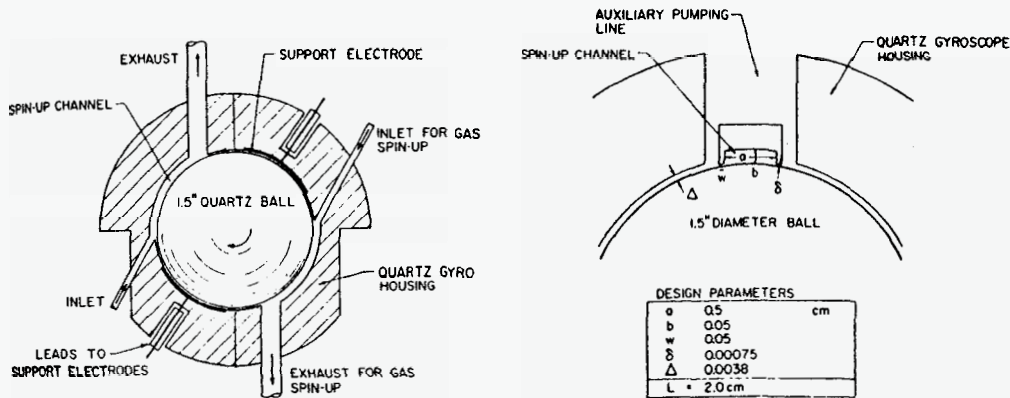

FIGURE 1. Cross-section of the gyroscope with details of spin up channel.

The gyroscope is illustrated in figure 1. It consists of a 1.5 inch diameter ball of extremely homogeneous fused quartz, ground and polished to a sphericity of better than 1 μin, and coated with a thin film of superconducting niobium. The ball is suspended within a spherical cavity by voltages applied to circular electrodes sputtered onto the inside wall of the housing. The suspension system uses ac support voltages and sensing signals as described below. On earth a field of about 700 V rms/mil must be applied to support the rotor. In space, with the gyroscope nearly in free fall, the support field is lowered to about 0.2 V/mil. The rotor is spun to its operating speed of about 170 Hz by means of a gas jet system shown

in the figure. After spin up, the pressure is reduced to about 10^{-10} torr using a technique described in a following paper by Turneaure, Cornell, Levine and Lipa, and the ball is allowed to coast freely. Its spin down time constant at 10^{-10} torr is about 3000 years. As the rotor is spun up, it develops a magnetic dipole moment, called the London moment, which is aligned parallel to its spin axis, and is maintained by the superconducting properties of the rotor coating. To obtain readout information, a superconducting pickup loop is placed around the rotor and connected to a SQUID magnetometer. Any change in the pointing angle of the dipole relative to the loop normal gives a signal in the magnetometer.

A theoretical analysis of gyro performance, described briefly below, has established that a gyroscope with drift rate significantly less than 1 milliarc-sec/year can be built with existing technology provided that a number of severe constraints on the gyroscope and its environment are met. The principal manufacturing constraints chosen for the gyroscope after making various tradeoffs are given in table 1. The roundness requirements on the rotor and housing come from an analysis of gyro suspension torques, plus the torque due to residual electric charge on the rotor. The requirements on homogeneity and coating uniformity come from an analysis of torques of two kinds: (i) the action of the residual acceleration of the spacecraft on a ball whose center of mass and center of geometry do not coincide (mass-unbalance torque), and (ii) the action of the gradient in the earth's gravitational field on the quadrupole mass-moment of the ball (gravity gradient torque). The two effects yield drift rates which set comparable limits on rotor homogeneity.

TABLE 1. MANUFACTURING TOLERANCES FOR THE RELATIVITY GYROSCOPE.

Sphericity of rotor	$<0.8\ \mu in$
Variation in thickness of rotor coating	$<0.3\ \mu in$
Rotor homogeneity	$\sim 3 \times 10^{-7}$
Sphericity of housing cavity	$<20\ \mu in$

3. GYRO ROTORS

There are four main steps needed to fabricate a rotor suitable for the gyro experiment. First, material of acceptable homogeneity must be selected. At

present this is done using interferometric techniques. Second, an accurate sphere must be cut. Next, it must be measured to a precision approaching 0.1 μin in roundness, and finally it must be coated with a robust, thin superconducting film. These steps are outlined briefly below.

Theoretical analysis and empirical evidence [2] establish a relationship between variations in the density ρ of transparent materials and variations in their refractive index n of the approximate form $\Delta\rho/\rho \sim 2.3\Delta n/n$. Hence, if one can measure variations in the refractive index of the fused quartz from which the rotor is to be made to about 1 part in 10^7, one can determine the density variations to the 3 parts in 10^7 requirement of table 1.

In 1979 J. Bates and M. Player at the University of Aberdeen commenced a program to develop an improved measuring instrument, initially for checking cubes but with the possibility of being adapted to make measurements on the finished rotors. The system measures optical path length using a laser interferometer. To avoid errors from surface irregularities, the cube is immersed in a cell containing a fluid mixture with a refractive index very nearly equal to that of the quartz. One beam of the interferometer is sent through the cell at a fixed location, and the cube is translated from side to side on a carriage immersed in the fluid. The total mechanical path length is a constant, being the sum of the distances through the cell windows, the fluid and the cube. The index-matching technique eliminates optical path length changes due to sample thickness changes, leaving only the contribution from the internal density variations. The second beam does not intersect the cube and is reflected from a fixed mirror to provide a reference path length. Figure 2 shows measurements obtained by Player
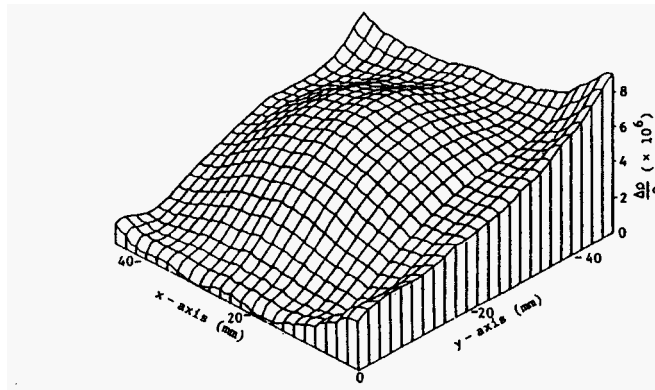

FIGURE 2. Refractive index variations across the face of a 2 inch quartz cube.

and Dunbar [3] of the integral refractive index variations parallel to one axis of a quartz cube. Similar maps were made for the other two axes. For this particular cube, the range of index variations across the face corresponded to density variation $\Delta\rho/\rho$ of 8×10^{-6}. To obtain full information on the density distribution within a cube, a tomographic method must be used, which is still under development [4]. In our case we are primarily interested in setting bounds on the low frequency density variations, so the integral path length data is acceptable. Material of much higher quality than that used for the preliminary measurements described here can be obtained. By the use of well-controlled precision anneal cycles, density variations as low as a few parts in 10^7 over rotor-sized areas have been reported [5].

Once the material is selected, it is rough ground to a spherical shape and then lapped and polished to the right diameter and sphericity. Since it is more convenient to fit the rotor to the gyro housing than the housing to the rotor, the sphere is brought to size to within about 20 μin. The diameter is controlled by monitoring the polishing rate. After many experiments, a lapping machine was designed by W. Angele [6], capable of routinely producing rotors with maximum peak-to-valley departures from sphericity of about 1 μin. The machine has four laps, arranged tetrahedrally, and is enclosed in a lucite box for cleanliness and temperature stability. The laps are all driven at the same speed, but their directions of rotation are reversed in a programmed sequence. An important step in achieving the final accuracy has been to develop an alignment procedure that makes the axes of rotation of the four laps coincide at the center of the ball to high precision.

To verify the sphericity of a rotor, a complete three-dimensional map of the surface of the sphere with an accuracy of about 0.1 μin is needed. Machines capable of measuring roundness to this precision in one plane have been available for a number of years. With the Talynova-73 computer-aided roundness measuring system we use, the workpiece is held fixed and the measurement is made with a rotating stylus transducer mounted on a precision spindle. To generate the data for complete maps of spherical rotors, we constructed a fixture which allows the ball to be turned through a succession of known angular increments about a horizontal axis. A series of great circle measurements on the ball is digitally processed to give either latitude-longitude maps or contour maps of the surface [7]. Figure 3 shows contour maps of a ball rotated in steps of 90° about the vertical axis. This rotor has a peak-to-valley maximum variation of about 2.4 μin. The information of most use in calculating gyro torques is the numerical value of each coefficient in a spherical harmonic expansion of the rotor shape. This too can be computed from the Talynova measurements [8].

The quartz rotor is coated with niobium to provide readout and suspension capability. If the coating is nonuniform, it will make the rotor
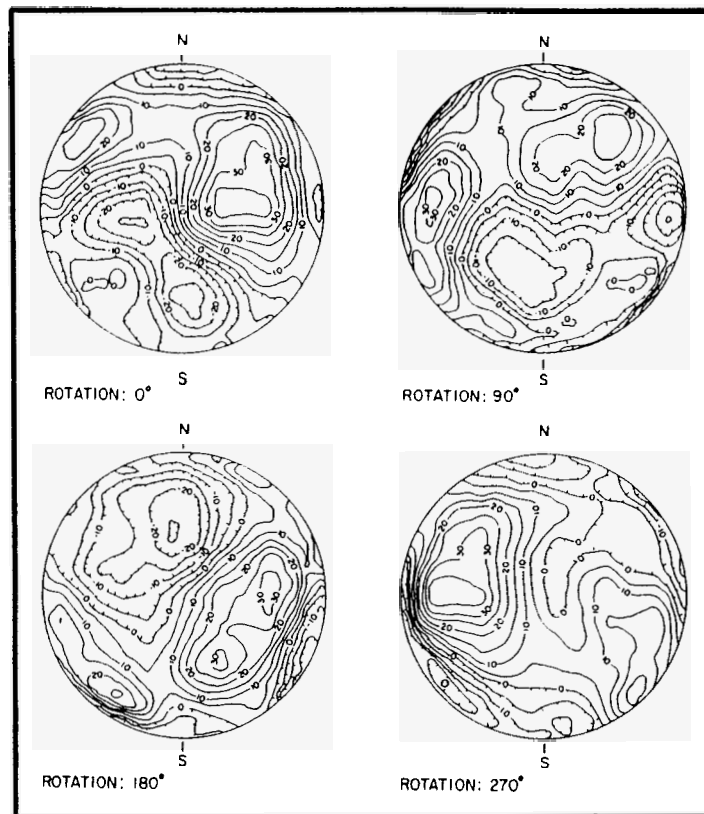
FIGURE 3. Contour maps of the surface of a quartz gyro rotor. Contour intervals are 5 nanometers, with tie-marks indicating areas below the mean surface level.

out-of-round, and because the density of niobium differs from that of quartz, it could also disturb its mass balance. A simple calculation shows that the requirement on mass balance sets a limit of 0.3 μin on the maximum peak-to-valley thickness variation that can be allowed. This in turn sets a limit on the thickness of the coating, depending on how uniformly it can be applied. To obtain a highly robust coating, the technique of sputter deposition is used. In this method a somewhat diffuse stream of niobium atoms is transferred from a target to the rotor. To obtain a uniform coating, the rotor must be rolled during the deposition to present all elements equally to the target. A number of techniques to do this were developed, the most successful to date using a microprocessor-controlled two-axis roller system. With such a device, a uniformity of about 2% has been achieved [9].

In early laboratory tests of the gyroscope, we encountered difficulty in levitating rotors with thin coatings owing to catastrophic electrical

breakdown at high voltage. The difficulty was partly a matter of cleanliness and partly a matter of adhesion; dirt in the housing and sharp edges around a puncture in the film (whether on the rotor or the electrode) would both cause breakdown. The problem was avoided by using coatings 100 μin thick. Such a coating would have to be uniform to 0.3% in both thickness and density to meet the requirements of the flight experiment. More recently we have been experimenting with the levitation of rotors with coatings in the 5–20 μin range. With the use of careful procedures aimed at reducing particle contamination we have now been successful in obtaining reliable long term operation with the thin films. To achieve this it was also necessary to improve the deposition technique substantially, and we were assisted by J. Siebert of Ball Aerospace in this area.

4. ROTOR SPIN UP AND HOUSING DESIGN

The gas jet system used to spin the rotor is shown schematically in figure 1. The rotor must be spun up while it is in the superconducting state in order to develop the London moment. The use of a cryogenic spin up system poses problems because of the very low viscosity of the helium gas, and its relatively short mean free path. These two factors dictate that the side walls of the spin up channel shown in the lower portion of the figure must approach to within 300 μin of the rotor. Without this narrow clearance it would be impossible to hold the pressure in the electrode area low enough to avoid both electrical breakdown and excessive drag while applying enough torque within the channel to reach the operating speed. On the other hand, the rotor-to-electrode gap must be large enough to reduce the torques on the gyro due to electrode imperfections to a tolerable level. With a 20 μin sphericity requirement on the electrodes, a gap of 1.5 mils to the electrodes is needed to meet the flight performance goal. Thus the raised ridges around a spin up channel are an essential feature of the design in figure 1. This detail of the design has a major influence on the techniques used to fabricate the housing.

By far the best method for making a spherical surface within a housing formed from two hemispherical shells is "tumble-lapping." In this procedure, first developed by Honeywell, two roughed out hemispheres are pinned together in their final configuration with a weighted lap and grinding compound in the cavity, and then shaken about two or more axes on a special vibration machine. Sphericities of 5 μin are achieved, allowing a 10–15 μin margin for the uniformity of the sputtered electrodes. Because tumble lapping is intrinsically a full sphere cutting procedure, it is necessary to form the raised ridges after the electrode surfaces are completed. Only two approaches are available for making the raised ridges after tumble lapping: deposition of metal or quartz on the ridges, or insertion of a

separate quartz piece containing the spin up channels. So far, the deposition technique has been used successfully only on housings made from alumina ceramic. Severe difficulties were encountered when quartz housings were used, due primarily to the brittle nature of the material. For laboratory testing a ceramic housing is acceptable, but questions exist concerning its shape at low temperatures. Thus, for the flight gyro, quartz and the insert approach are used.
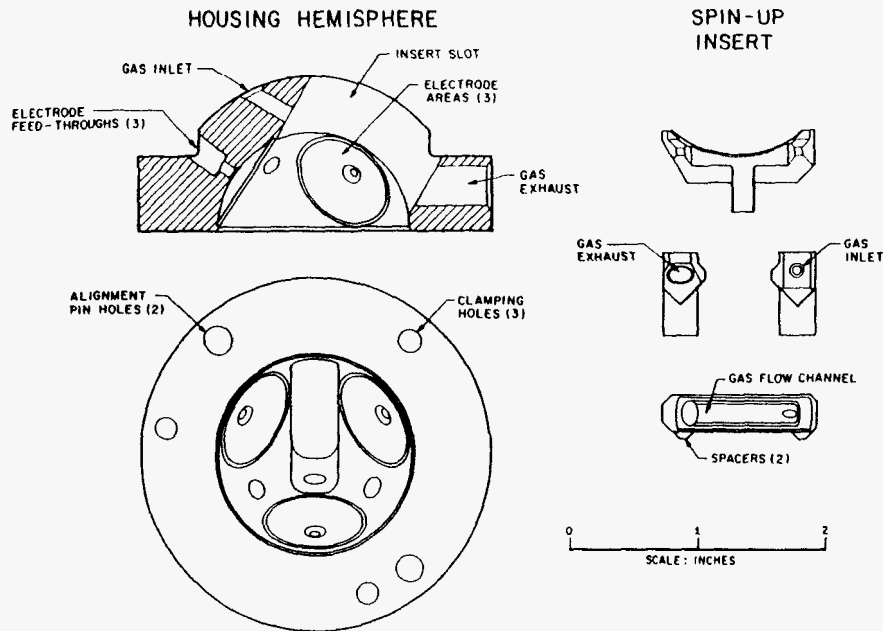

FIGURE 4. Design of quartz housing with inserts.

Figure 4 shows the design of a quartz housing with inserts. In this design each spin up channel is fabricated as a single unit, independent of the gyro housing, and glued laterally to the walls of a slot cut through the housing. The most critical problem is cementing the pieces together in such a way that they are aligned within a 50 μin tolerance and can withstand repeated cycling to low temperatures. Quartz wedges (not shown) are used to hold the insert away from the wall of the slot opposite the insert spacers, and the correct elevation of the ridges above the electrode surface is established by cementing the inserts into place with the housing temporarily assembled and containing a wedged-in tooling ball of radius 300 μin greater than the radius of the gyro rotor. This housing meets all the requirements for a flight gyroscope.

During the course of gyro testing it proved important to have accurate centering adjustments on each axis of the electrical suspension system. The ability to move the ball precisely to any position in the housing suggests a variant method of spin up. Instead of passing gas through two balanced channels with raised lands, one makes use of a single channel without raised lands and moves the ball towards that channel, temporarily reducing the rotor-housing gap Δ to the value δ required for spin up. Although the use of only one channel halves the area of gas in contact with the ball, the ultimate spin speed can remain the same because the drag in the housing can be reduced by a similar factor. Single channel spin up allows a simpler housing design. Also, it allows one to maintain a larger rotor-electrode gap during normal gyro operation. Small raised pads in the housing prevent the ball from sitting directly on the electrodes.

Optimization of a single channel system follows similar lines to that of a dual channel system [10]. One difference is that there is an upper limit on the channel length. Since the rotor and housing are of different radii, the rotor-land gap for the translated rotor is not uniform. Simple geometric considerations show that if the half-angle subtended by the channel at the center of the rotor exceeds 30°, gas leakage at the ends of the channel will become excessive. A redesign for a significantly shorter channel could allow an increase of up to 20% in electrode area, which is good. With a shorter channel, the momentum transfer efficiency is reduced, so even though the gas pressure (and hence the mass throughput) is higher, the gyroscope takes longer to spin up. With a 5% efficiency, the mass of helium needed is about 250 g per gyro. Although the gas pressure is higher than with dual channel spin up, the reduction in channel area makes the lateral acceleration exerted by the gas on the ball acceptable, certainly less than 0.2 g. We have demonstrated single channel spin up in existing housings, and are designing a new housing with a configuration close to the optimum.

5. ROTOR SUSPENSION

The suspension system used in ground-based testing of the gyroscope was designed by the late J. R. Nikirk, following principles applied in the Honeywell gyroscope. Suspension is by 20 kHz voltages applied to the three pairs of electrodes, in the form of a constant or "preload" component and a variable or "control" component. The control voltage is added to one electrode and subtracted from the opposite electrode to generate a net force along the given axis. This approach linearizes the system; the force, even though it depends on the square of the voltage, is directly proportional to the control component. The rotor is maintained at zero voltage by making the system three-phase, each phase being associated with one of the three orthogonal support axes. The position of the

rotor in the housing is measured by applying 1 MHz sensing signals to the same electrodes as are used for support. Opposed pairs of electrodes form two arms of a capacitance bridge; the unbalanced output from the bridge serves as the control signal for adjusting the 20 kHz support voltages. The control bandwidth is 4000 rad/sec. The voltage needed to support the ball on earth with a 1.5 mil rotor-electrode gap is about 1 kV rms. With a sensing voltage of 3 V, the centering accuracy is better than 1 μin.

Paper VI.3(E) by R. Van Patten describes the extension of this concept to a multilevel suspension system for use in the actual flight experiment.

6.   LABORATORY TESTING

The first cryogenic gyro test facility was completed in 1973 and used for general gyro testing, spin up demonstration, London moment observations and simple gyro dynamics studies. A schematic view of the apparatus is shown in figure 5. The dewar was equipped with two layers of conventional magnetic shielding to achieve a residual field of about 10^{-5} gauss after
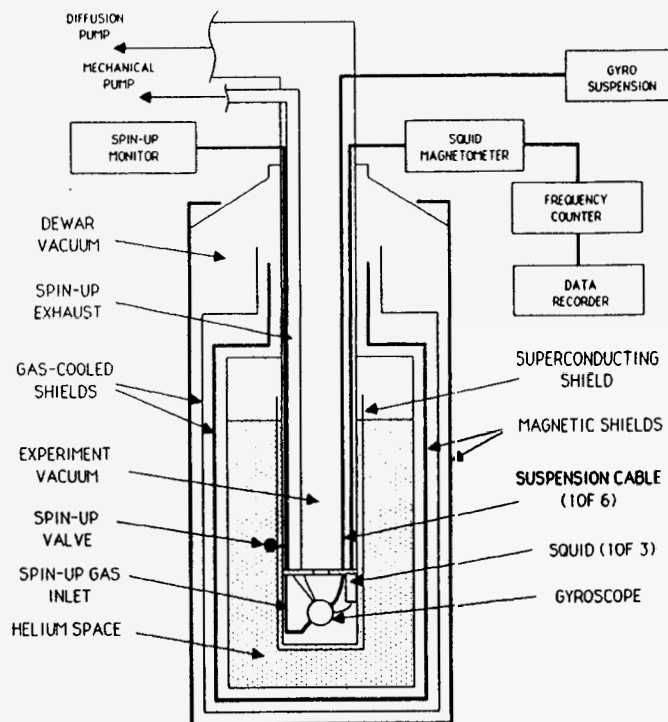

FIGURE 5. Schematic view of first gyro test facility.

careful adjustment of the remanent magnetization, and with a supercon-
ducting shield to stabilize the field after cool down. Spin up was performed
with the dual channel system described above and readout with a three-axis
SQUID magnetometer system fabricated by R. Clappier and J. Anderson.
Because of the relatively high level of background field, it was difficult to
use the London moment as a readout of the spin axis direction, and obser-
vations [11] were confined to measurements of its amplitude as a function of
spin speed. On the other hand, the trapped flux from the background field
could independently be used to observe not only the motion of the spin
axis as a function of time but also the motion of the body axes relative to
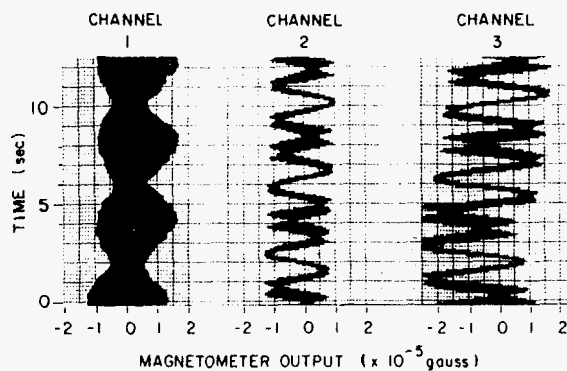the spin axis, the polhoding motion.

FIGURE 6. Trapped flux signals from a gyro rotor undergoing precession

An example of the type of output obtained from the trapped flux signal
is shown in figure 6. The left hand trace shows the output observed with
a pickup loop in the horizontal plane, with time running upward, and the
other two traces show signals from the two orthogonal loops with their
planes vertical. The high frequency signal is due to the rotation of the
trapped flux around the spin axis at the spin speed. In the center and
R.H. traces, this signal is modulated by an intermediate frequency which
is 90° phase shifted between the loops. This corresponds to a precession
of the spin axis. Since this signal is not present in the L.H. trace, we can
conclude that the motion is confined to precession about the vertical axis,
similar to a simple top. The L.H. trace shows a strong modulation at an
even lower frequency, and a similar effect can be seen on the other traces.
This signal is in phase on all three channels and corresponds to the polhode
motion of the spin axis relative to the rotor body axes. Thus one can see
that the trapped flux signal is a simple and powerful tool for studying the

dynamical behavior of the gyroscope. However it is not easy to turn this signal into a precision readout suitable for the relativity experiment. For this we need the full London moment readout.
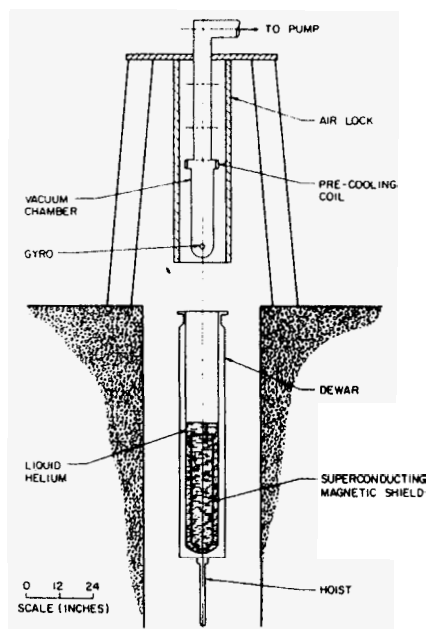

FIGURE 7. Low magnetic field gyro test facility.

In 1975 we decided to build a new apparatus in which the gyroscopes would be placed in an ultralow magnetic field shield made by the techniques described by B. Cabrera elsewhere in the volume. This apparatus [12] is shown in figure 7. The gyroscope is mounted on a support structure hanging inside an experiment chamber that can be exhausted to a pressure of a few times 10^{-7} torr. The top plate of the chamber is attached to a rigid frame which stands on a concrete isolation pad in order to provide a very stable mount for the experiment. A helium dewar, kept permanently cold, contains the ultralow magnetic field shield. The dewar can be raised and lowered on a hydraulic piston and used to cool the apparatus to cryogenic temperatures. An airlock prevents solid air from condensing into the dewar while it is being lifted into the operating position.

Two types of rotors have been studied in the low field test facility, a quartz rotor and a hollow beryllium rotor. This latter rotor is of the Honeywell type with a 10% difference in moments of inertia, but coated with

a superconducting film to allow readout. With the large moment of inertia ratio, the polhode frequency is about 10% of the spin speed, and thus can easily be placed far above the precession frequency. Simple filtering techniques can then be used to eliminate the ac trapped flux signal from the magnetometer outputs, suppressing both the spin speed signal and the polhode signal. In figure 8 we show the resultant signal, of which a few
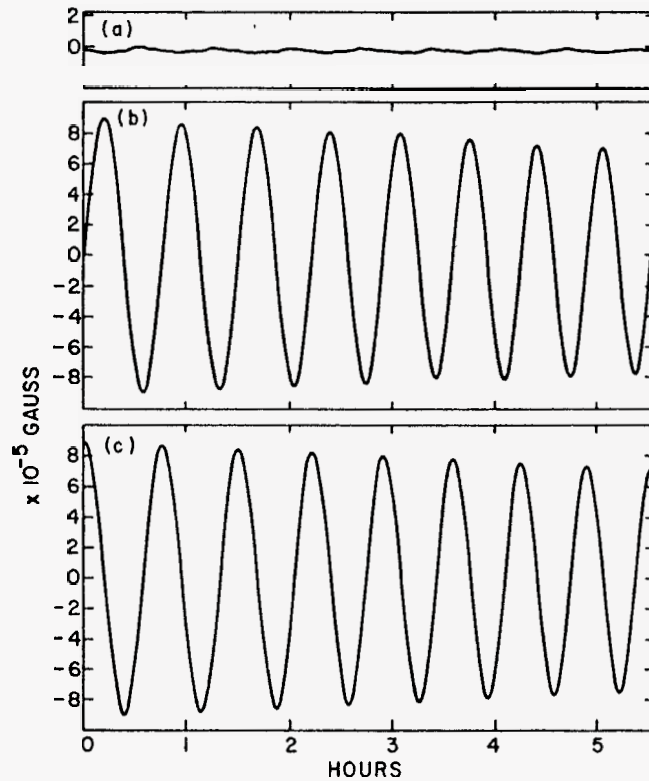

FIGURE 8. London moment readout signals with hollow beryllium rotor

percent is due to dc trapped flux and the remainder due to the London moment. The upper trace is the signal from a loop with its plane horizontal and the other two from crossed loops with their planes vertical. Again the precession signal is primarily due to spin axis motion about the local vertical. With this system we have obtained an angular resolution equivalent at a 200 Hz spin speed to about 1 arc-sec in a 10 sec integration time, in agreement with that expected from magnetometer noise considerations. In

most of the tests the gyro rotor has had a large mass unbalance, principally because with the thick rotor coatings it is not easy to get a well-balanced ball, but also because it is convenient in developmental work to take advantage of the rapid precession of the gyroscope about the vertical axis caused by the mass-unbalance torque.
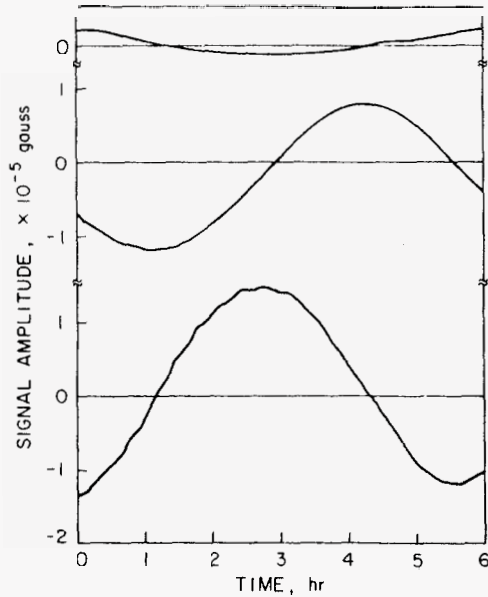

FIGURE 9. London moment readout signals with quartz rotor.

In figure 9 we show the readout signals obtained with a quartz rotor. Here the polhode frequency is of necessity very low and it cannot readily be filtered from the data. The single sine wave is due to precession and the "ripple" to polhoding. The London moment, again comprising the bulk of the signal, does not give rise to the polhoding signal; it is due to modulation of the residual trapped flux. This record shows significantly more noise than that in figure 8. This is due primarily to the use of a five times heavier rotor and the related increase in the suspension system output voltages. Extensive shielding of the magnetometer input circuit is necessary to reduce pick up from the suspension system to an acceptable level. Of course for the flight experiment this source of interference will be negligible, due to the low support forces applied in the close-to-free fall environment of the spacecraft. The upper trace contains a noticeable component of the basic precession sine wave. This is probably due to the effect of the earth's rotation on the precession.

7. TORQUE ANALYSIS

Gyro torques may be divided into two classes: (i) support-dependent, (ii) support-independent. The support-dependent torques include the mass-unbalance torque and the torques from the suspension system acting on the out-of-roundness of the gyro rotor. The support-independent torques include the various effects of gravity gradients, electric charge on the rotor, magnetic fields, residual gas, cosmic rays, photon bombardment, all of which are negligible in an earth-based gyroscope and therefore need careful study to make sure that they can be held below the 0.3 milliarc-sec/year design goal of the experiment.

Equation (1) in the previous paper shows that the mass-unbalance torque is proportional to the residual acceleration transverse to the gyroscope spin axis multiplied by $\delta r/r$, the ratio of the displacement between center of geometry and center of mass to the radius of the gyro rotor. Assuming a uniform density gradient from one pole of the spinning ball to the other, $\Delta r/r$ may be replaced by $3/8\ (\delta\rho/\rho)$, where $\delta\rho$ is the difference between the densities at the two poles. If, to obtain a gyroscope with a drift rate below 0.3 milliarc-sec/year, we stipulate that no individual torque term shall contribute an error greater than 0.1 milliarc-sec/year, then we find that the requirement on density is $\delta\rho/\rho < 3 \times 10^{-7}$, **as given in table 1.**

Recently [13] analysis has greatly improved and simplified the evaluation of support-dependent torques by expanding the shape of the rotor in spherical harmonics, and calculating the torque from the differential with respect to angle of the energy stored in the support field. The calculation is effected with the aid of the D-matrices used in nuclear physics to rotate a set of spherical harmonics from one system of coordinates to another. The expression for the primary torques depending only on rotor shape is

$$\Gamma_n = -\frac{\partial}{\partial\eta} \sum_{\ell p} C'_{\ell p} B_{\ell o} Y_{\ell p}(\beta,\alpha) \quad , \tag{1}$$

where η is the rotation angle, the $Y_{\ell p}$ are spherical harmonics, the $B_{\ell o}$ are coefficients in the expansion of the rotor out-of-roundness in the rotor coordinate frame, and the $C'_{\ell p}$ are coefficients which express the demarcation of the electrode boundaries in terms of a spherical harmonic expansion in the housing coordinate frame, separately summed over the squares of the voltages applied to the six electrodes. The only integration needed to reduce equation (1) to numerical form is the one to find the $C'_{\ell p}$, and this integration may be done by hand from a table of Legendre polynomials.

When the results from the primary suspension torques are translated into expressions giving the drift rate Ω of the gyroscope in terms of applied acceleration, they reduce to two forms, one for odd and one for even

harmonics of the rotor shape. If the suspension system is assumed to have a fixed preload and the gyro spin vector is assumed to point (as it will very nearly do in space) along a line in the y-z plane lying exactly midway between two electrodes whose axes are labeled y and z, the resulting expressions may be written

$$\Omega_p^{\text{odd}} = \frac{f}{v_s} \sum_{\ell \text{ odd}} B_{\ell_o} A_\ell \tag{2}$$

$$\Omega_p^{\text{even}} = \left[\zeta h + \frac{f_z^2 - f_y^2}{h} \right] \sum_{\ell \text{ even}} B_{\ell_o} A_\ell' . \tag{3}$$

In these equations v_s is the peripheral velocity of the rotor, A_ℓ, A_ℓ' are numerical coefficients, h is the "preload acceleration," $i.e.$, the acceleration that has to be applied parallel to an electrode axis to drive the voltage on the opposite electrode to zero, f_z and f_y are components of acceleration parallel to the z and y electrode axes, and $\zeta = (h_z - h_y)/h$ is the preload compensation factor, a numerical coefficient expressing the extent to which the preloads in different axes are matched. The equation for odd harmonics is identical in form to the equation for the mass-unbalance torque; the equation for even harmonics involves the preload acceleration also.

To reduce equation (2) to numerical predictions, one needs to know the structure of the acceleration $\mathbf{f}$ acting on the gyroscope, which is made up of four terms: $\mathbf{f} = \mathbf{f}_d + \mathbf{f}_c + \mathbf{f}_g + \mathbf{f}_\nu$, where $\mathbf{f}_d$ is the limit on the dragfree controller, $\mathbf{f}_c$ is the centrifugal acceleration due to spacecraft roll, $\mathbf{f}_g$ is the gravity gradient acceleration which arises from the gyroscope's not being at the center of mass of the spacecraft, and $\mathbf{f}_\nu$ is the acceleration produced by noise in the pointing servo. For odd harmonic torques and the mass-unbalance torque, one takes averages of the accelerations; for even hormonic torques, one has to take into account the possibility of rectification from the squared terms f_z^2 and f_y^2 in equation (3).

The centrifugal acceleration $\mathbf{f}_c$ is well averaged by roll in its effect on both odd and even harmonics; however, it has been shown that the slight misalignment of the gyro spin vector with the spacecraft roll axis gives rise to a small torque from the preload term h in equation (3), in consequence of which for a preload of 10^{-6} g the average position of the gyro spin vector over the year has to be held to within about 10 arc-sec of the roll axis. For a 10^{-7} g preload, the alignment can be correspondingly relaxed.

The noise acceleration $\mathbf{f}_\nu$ is surprisingly large, about 3×10^{-6} g at the 25 rad/sec bandwidth of the inner loop of the pointing servo. However, most of the noise comes in above the 4 rad/sec bandwidth of the suspension system and has no effect on the gyroscope. Also, the drift rate from the residual effect comes only through the misalignment of the gyro spin vector. The magnitude is at most 10^{-2} **milliarc-sec/year.**

For the gravity gradient term, we consider a gyroscope displaced from the center of mass of the spacecraft through a distance ℓ along the roll axis. In a satellite moving in a near-circular orbit, and having its roll axis misaligned with the orbiting plane by an angle α, the acceleration $\mathbf{f}_g$ is

$$\mathbf{f}_g = \frac{g'\ell}{2R}\left[(1 + 3\cos 2\omega_o^t)\mathbf{n}_\ell + 3\sin 2\omega_o^t\mathbf{n}_p + \alpha\mathbf{n}_o\right] , \qquad (4)$$

where R is the radius of the orbit, g' is the earth's acceleration at orbit altitude, ω_o^t is the mean motion, and $\mathbf{n}_\ell$, $\mathbf{n}_o$ and $\mathbf{n}_p$ are unit vectors in directions respectively parallel to ℓ, along the orbit normal, and in the orbit plane perpendicular to both ℓ and the orbit normal. For an ℓ of 20 cm, the quantity $g'\ell/2R$ is about 1.5×10^{-8} g. Thus in the orbit plane there is a secular acceleration parallel to ℓ (and therefore nearly parallel to the gyro spin vector) of magnitude 1.5×10^{-8} g, and a cyclic term rotating at twice the orbital rate, of amplitude 4.5×10^{-8} g. Perpendicular to the orbit plane there is a secular term of magnitude 1.5×10^{-8} αg, which with an α of 2° would yield 10^{-9} g. The secular term is in the direction $\mathbf{n}_\ell$, and though large in comparison with the 10^{-10} g residual acceleration $\mathbf{f}_d$ from the drag free controller, has negligible effect on the gyroscope since it is nearly parallel to the gyro spin vector. The cyclic acceleration term averages over the orbit for odd harmonics in the shape of the rotor, and averages over the combination of roll and orbit for the even harmonics. Only the secular term perpendicular to the orbit plane is significant. It yields a torque proportional to α which causes a precession of the gyroscope in the orbit plane, i.e., in the same plane as the geodetic precession. Since in a regressing orbit α changes linearly with time, the resultant drift rate will be quadratic in time, so that even if α is large enough for the term to introduce a significant error in the measurement of the geodetic precession, the error can be removed in data reduction.

Summing up the argument, we find that the only terms in $\mathbf{f}$ that are significant are the component of gravity gradient acceleration $(g'\ell\alpha/2R)\mathbf{n}_o$ along the orbit normal and the component of residual acceleration $(\mathbf{f}_d)_i$ from imperfect dragfree performance left in inertial space perpendicular to the roll axis after allowing for any averaging from the roll. The gradient term is known exactly once the orbit is known. For the residual drag we make the conservative assumption that $(\mathbf{f}_d)_i$ is 10^{-10} g, i.e., that there is no significant benefit from roll. Once the accelerations are known, upper limits on the drift rates of the gyroscope due to mass-unbalance and primary suspension torques may be calculated from the known limits on homogeneity and out-of-roundness, together with the known preload and the average misalignment of the gyro spin vector. The conclusion of the analysis is that drifts of the gyroscope due to mass-unbalance and suspension torques can both separately be held below 0.1 milliarc-sec/year.

TABLE 2. SUMMARY OF GYROSCOPE DRIFT ERRORS.

Torque	Drift Rate (milliarc-sec/year)
Mass unbalance	<0.1
Suspension:	
Primary	<0.1
Secondary	<0.03
Gravity gradient	<0.05
Magnetic:	
Direct	$<10^{-5}$
Differential damping	$<10^{-8}$
Electric:	
Charge on ball	<0.001
Patch effect	<0.01
Gas:	
Differential damping	<0.1
Brownian motion	$<6 \times 10^{-5}$
Photon bombardment	$\sim 10^{-6}$
Cosmic rays:	
Primary (iron nuclei)	$<10^{-3}$
South Atlantic anomaly	$\sim 4 \times 10^{-4}$
Showers from sun	$\leq 4 \times 10^{-4}$
Worst-case-sum	<0.38
Root-mean-square sum	<0.18

The support-independent torques have been treated exhaustively elsewhere [14]. Table 2 gives upper limits on the principal drift terms for a gyroscope in a satellite moving in an orbit with coinclination 10 arc-min.

References

[1] As quoted by H. W. Knoebel, *Control Engineering* **11**, 70 (1964). Earlier reports are not widely available.

[2] G. J. Siddall, private communication.

[3] M. Player and G. Dunbar, private communication.

[4] L. V. de Sa, Thesis, University of Aberdeen (1981).

[5] I. M. Siddiqui and R. W. Smith, *Optica Acta* **25**, 737 (1978).

[6] W. Angele, *Prec. Engr.* **2**, 119 (1980).

[7] J. A. Lipa and J. Bourg, *Prec. Engr.* **5**, 101 (1983).

[8] J. A. Lipa and G. J. Siddall, *Prec. Engr.* **2**, 123 (1980).

[9] P. Peters, private communication.

[10] T. D. Bracken and C. W. F. Everitt, *Adv. Cry. Eng.*, **13**, 168 (1968), and G. R. Karr, J. B. Hendricks and J. A. Lipa, *Physica* **107B**, 21 (1981).

[11] J. A. Lipa, J. R. Nikirk, J. T. Anderson and R. R. Clappier, *LT-14 Proceedings* (North-Holland, Amsterdam, 1975), Vol. 4, p. 250.

[12] B. Cabrera and F. J. van Kann, *Acta Astronautica* **5**, 125 (1978).

[13] G. M. Keiser, to be published.

[14] "Report on a Program to Develop a Gyro Test of General Relativity in a Satellite and Associated Control Technology," edited by C. W. F. Everitt (HEPL, Stanford University, 1980), p. 560. Contributors: J. T. Anderson, J. V. Breakwell, B. Cabrera, R. R. Clappier, D. B. DeBra, P. Eby (NASA Marshall Center), J. J. Gilderoy, Jr. , G. M. Keiser, B. C. Leslie, J. A. Lipa, G. J. Siddall, F. J. van Kann, R. A. Van Patten and R. Vassar.